



Correlation Between Surface Morphology and Optical Properties of Quasi-Columnar Porous Silicon Nanostructures

S. Rasi, N. Naderi*, M. Moradi

Department of Semiconductor, Materials and Energy Research Center, Karaj, Iran

PAPER INFO

Paper history:

Received 25 December 2016

Accepted in revised form 30 April 2017

Keywords:

Optical Properties
Porous Silicon
Morphology
Current Density
Porosity

ABSTRACT

In the current work, the effect of surface morphology on light emission property and absorption behavior of quasi-columnar macro-porous silicon (PS) was investigated. PS structures with different morphology were synthesized using photo-electrochemical etching method by applying different etching current densities. SEM micrographs showed that empty macro-pores size and porosity of PS layers were increased by increasing the current density which is due to passivity breakdown in initiated pore walls. Also, a decrease in pores density and a diminishing of nanocrystallites density on PS samples surface was observed for the samples with higher etching current densities and porosity. We conclude that porosity is not necessarily increased in order of forming more pores and formation of more nanocrystallites in PS structures. By increasing etching current density, a red shift in Raman peak position of PS samples was observed which was due to the residual stress and quantum confinement (QC) effects on the PS structures. PL peak position was also shifted to higher frequencies which is in good agreement with Raman red shift due to QC effect on finite size crystallites. Maximum PL intensity was observed for the sample with higher pore density and smaller pore size. Although the PS structure with maximum pore size had the maximum porosity, but it showed a remarkable decrease in PL intensity because of trapping of irradiated light in quasi-columnar empty macropores. Therefore, porosity is not the only factor having effect on optical properties such as photoluminescence efficiency. The morphology and size of pores can also be outstanding parameters responsible for variation of optical behavior of PS nanostructures.

1. INTRODUCTION

Due to extremely large surface-to-volume ratio up to 200–500 m^2cm^{-3} [1], surface roughening and excellent physical properties such as tunable broad direct band gap and efficient visible room temperature luminescence properties [2], PS is a material of interest in many applications such as solar cells and photodetectors [3-5].

Electrochemical etching technique is a well-controlled and attractive technique for fabrication of uniform pores on the surface of silicon substrates because of its capability to control the etching rate by optimizing several parameters such as etching current density, etching time, and ratio of chemicals in solution [6].

It is well known that etching current density is one of the most effective parameters for controlling the morphology and porosity of PS nanostructures [7-9]. Hole supply by Si is the necessary initial step of the electrochemical dissolution process. Under anodic

polarization, holes are supplied by Si. For the fabrication of luminescent PS from n-type Si, generation of hole is generally performed by illumination [10].

Several investigations have shown that the optical characteristics of PS may considerably change upon porosity variation [11, 12]. In general, a highly porous layer has high photoluminescence (PL) efficiency due to presence of more luminescent Si nanocrystallites on the surface [13].

Also, light absorption can be enhanced by increasing porosity due to light trapping in PS layer [13-15]. Light trapping in PS structures can reduce PL efficiency due to capturing the irradiated light in PS walls. Thus, it seems that the porosity of PS layer cannot be the only effective parameter determining the optical properties. In this report, in order to clear the role of porosity and other structural parameters in optical properties, variation in light emission and light trapping properties of PS layers with different porosity and morphology is studied.

*Corresponding Author's Email: n.naderi@merc.ac.ir (N. Naderi)

2. EXPERIMENTAL DETAILS

PS samples were synthesized by photo-assisted electrochemical etching (PECE) of (100) oriented phosphorus doped crystalline silicon (c-Si) substrates with resistivity of $0.05 \Omega \cdot \text{cm}$ and thickness of $680 \mu\text{m}$. A thin film of silver (Ag) with thickness of $\sim 150 \text{ nm}$ was deposited on the back side of c-Si substrates in order to facilitate anodization process. The metallization was taken place in a vacuum chamber of a sputtering system and an ultrapure Ag plate was used as a target. This process decreased the surface resistivity to $1 \text{ m}\Omega \cdot \text{cm}$ after 15 min annealing in tube furnace at 430°C under nitrogen gas flow.

Fig. 1 shows a schematic diagram of the two electrode PECE cell in which platinum mesh was used as cathode and was located approximately 10 mm above the surface of c-Si sample (anode). In order to provide the required holes for dissolution reactions on Si surface, the front side of the c-Si was exposed to a 100W tungsten lamp at a distance of 20 cm above it during the etching process. Current controlled etching process was applied due to simplicity of this technique and the constant rate of hole creation that leads to better uniformity in PS.

The used chemical solution contains a mixture of hydrofluoric acid (HF 38-40% w/w purchased from Merck Chemical Co.) and ethanol ($\text{C}_2\text{H}_5\text{OH}$ 96% w/w purchased from Merck Chemical Co.) in volume ratio of 1:4. Current densities as critical experimental parameters were fixed at 10, 20, 40, and $80 \text{ mA}\cdot\text{cm}^{-2}$ for sample *a*, *b*, *c* and *d*, respectively, using a DC SourceMeter (Keithley 2400) throughout the etching time (20 min). Immediately after the etching process, samples were taken out from the cell, rinsed in deionized water and ethanol, and then dried in nitrogen flow to ensure that all solutions have been evaporated. The surface of the etched samples appeared yellowish and showed visible light (orange) emission under 365 nm UV illumination which verifies formation of PS nanostructures. The surface morphology and structure of PS samples were characterized using Scanning Electron Microscope (SEM, Tescan Vega-3 LMU). Raman scattering of the samples was recorded at RT using a micro-Raman set-up (SENTERRA (2009) BRUKER) equipped with a laser diode source (excitation wavelength: 785 nm, 1mW, spectral resolution: $<3 \text{ cm}^{-1}$). The PL spectra measurements were carried out using a fluorescence spectroscopy setup (Avantes) equipped with a blue emission (405 nm, 20 mW) laser diode source for excitation. The optical reflectance of the PS layers were obtained using a visible light optical reflectometer (Filmetrics, F20) with power of 5mW from Xenon light source. Porosity percentage of the synthesized PS samples was calculated using gravimetric measurement with PS corrosive solution (KOH 3%) according to Equation (1):

$$P(\%) = \frac{m_1 - m_2}{m_1 - m_3} \times 100 \quad (1)$$

where, m_1 is the Si sample weight before etching process, m_2 is the sample weight after PS formation, and m_3 is the sample weight after removing the PS layer with a corrosive solution [13].

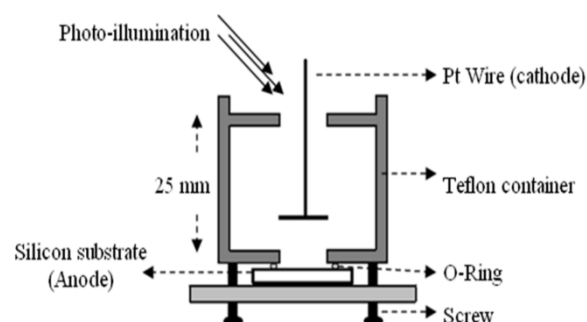


Figure 1. Schematic diagram of photo-electrochemical (PECE) etching cell

3. RESULTS AND DISCUSSIONS

Morphology of the synthesized PS layers with different applied etching current densities ($10, 20, 40,$ and $80 \text{ mA}\cdot\text{cm}^{-2}$) in the identical PECE conditions was characterized using SEM images (as shown in Figure 2). Fig. 2(a) shows formation of small macropores on the c-Si at $J = 10 \text{ mA}\cdot\text{cm}^{-2}$ and rougher surface compared to the c-Si, while star-like pores were not clearly observed. Maximum pore diameter obtained in this condition was about 200 nm. Figure 2(b) illustrates creation of stare-like pores and an increase in number of pores on the walls which have resulted in increase in porosity in comparison to sample *a*. The percentage of porosity for different PS samples which was calculated by gravimetric measurements is shown in Table 1. Planar view of samples *c* and *d* reveals higher porosity with substantially wider stare-like pores (with diameter of $\sim 1-4 \mu\text{m}$) in comparison to sample *b* (Figure 2(c) and (d)). The pores appear pitch black to the eye. SEM results clearly reveal that by increasing applied current density from 20 to $80 \text{ mA}\cdot\text{cm}^{-2}$, empty star-like macropore diameter of PS samples increases and pore density (number of the pores per unit area) decreases. Also, a diminishing of nanocrystallites density (total volume of Si nanocrystallites per unit area) was observed in SEM images (see Figure 2). Pore diameter enlargement can be due to the passivity breakdown in pore walls in higher current densities. In constant-current density, the rate of holes which are supplied to the Si anode surface is fixed. When number of the offered holes is more than that of the consumed holes at the tip, they start to penetrate into the pore walls and dissolution takes place on the surface of the pore walls [16]. Consequently, the pore diameter increases and the pores wall thickness reduces.

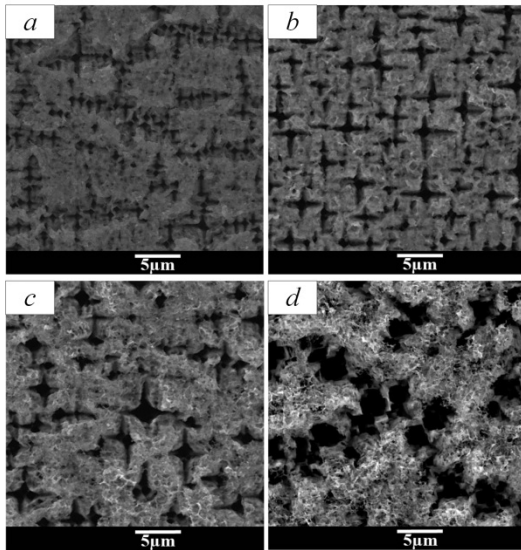


Figure 2. SEM micrographs of porous silicon samples with different current densities of 10, 20, 40, and 80 mA.cm⁻², respectively

Fig. 3 shows cross-sectional SEM images of the prepared PS samples. The interface of c-Si and PS is clear due to difference in their structures. It is observed that the thickness of pores perpendicular to the surface rises from 19 to 84 μm with increase in applied etching current density despite the same etching time for all PS samples. In the same etching condition, thickness of PS layer increases with etching time while etching rate is associated with amount of PECE condition. For proceeding the etching process, the electrolyte (especially HF) must fill the pores. However, when the pores are small, some will be filled with hydrogen gas, rather than liquid, at least near the tips of the pores.

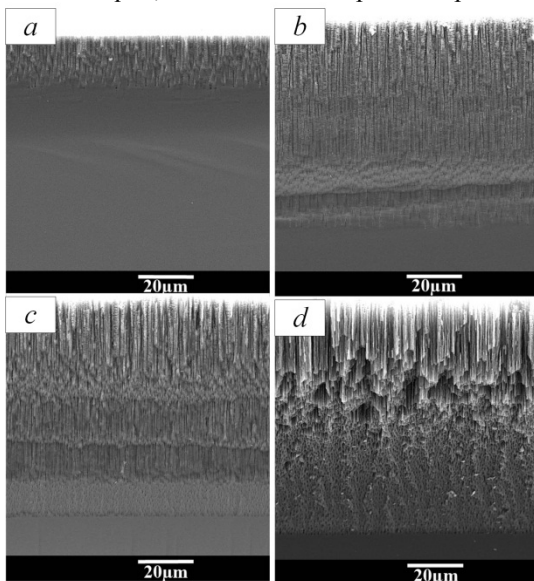


Figure 3. Cross-sectional SEM micrographs of porous silicon samples with different current densities of 10, 20, 40, and 80 mA.cm⁻², respectively

Increase in pore size allows fresh HF electrolytic solution to fill the pores easier, allowing the pores to grow perpendicular to the surface in a quasi-columnar porous structure. Therefore, in spite of constant etching time different thicknesses were observed for different current densities.

The pores in samples *a*, *b*, and *c* have straight depth. The cross-sectional image related to sample *d* demonstrates non-parallel and partially cracked silicon walls. Moreover, structural damage is observed in pores interconnection in planar view of this sample (Fig. 2(d)). The induced compressive stress in sample *d* could be as a result of high atomic mismatch between c-Si and PS structures which forms cracks and damages in this sample.

Other structural properties of the PS samples such as crystallites size and stress evolution are studied using Raman molecular spectroscopy. Effects of these two parameters are reflexed in Raman spectra in a same manner so that distinguishing between their effects is difficult [17]. Therefore in order to fully describe Raman properties in PS samples, effect of stress on nanocrystals should be taken into account.

The Raman spectra were recorded with excitation wavelength of 787 nm and laser power of 1mW (to avoid laser heating of the sample that can cause Raman shift [18]) at room temperature. Fig. 4 shows the Raman spectra of the PS samples compared with c-Si substrate. Momentum conservation in c-Si results a narrow peak at ~519cm⁻¹.

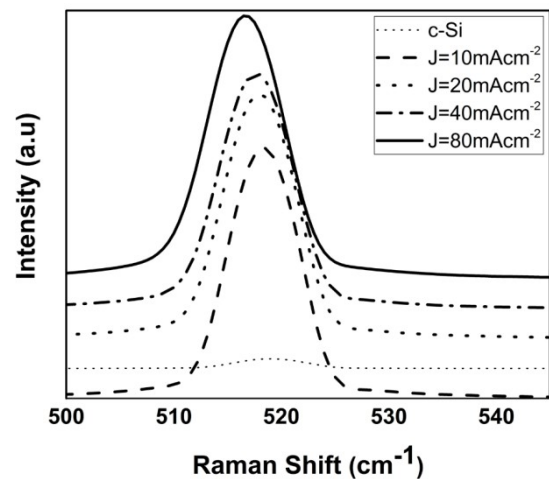


Figure 4. Raman spectra of porous silicon samples with different current densities of 10, 20, 40, and 80 mA.cm⁻² for samples *a*, *b*, *c* and *d*, respectively. The c-Si spectrum is shown for comparison

For PS samples, a Raman red shift with respect to the c-Si was observed from 519 to 516.5 cm⁻¹ along with an increase in full width at half maximum (FWHM) of the peaks that can be related to phonon confinement effect; In nanocrystals, phonons are localized in small

crystallites and the momentum is no longer well defined, which according to the uncertainty principle, enables phonons with momentum of $q \neq 0$ to contribute the Raman process. Thus PS show asymmetric broadening and a red shift to lower wavenumbers due to the phonon confinement effect [19].

TABLE 1. The phonon modes detected in the Raman spectra of the porous samples with different etching current densities

Sample s	J (mA.cm ⁻²)	P (%)	ω_{PS} (cm ⁻¹)	$\Delta\omega$ (cm ⁻¹)	L (nm)
a	10	34	518.5	0.5	10.2
b	20	39	518.0	1.0	6.6
c	40	43	517.5	1.5	5.1
d	80	57	516.5	2.5	3.7

The crystallite size of PS samples was estimated using Equation (2) and (3) which was shown by Paillard et al.:

$$\Delta\omega = A \times \left(\frac{a}{L}\right)^\gamma \quad (2)$$

$$\Delta\omega = \omega_{PS} - \omega_{Si} \quad (3)$$

where, a is the lattice constant of Si, L is the crystallite size, A and γ are used to describe the vibrational confinement due to the finite size in a nanocrystal and are dependent on the studied system. Based on Equation (2), increase in Raman red shift ($\Delta\omega$) is due to decrease in crystallites size (L). The estimated crystallite size of PS samples is listed in Table 1, It is shown that an increase in etching current density results in reducing crystallite size in PS samples.

The tensile and compressive stress in PS structure cause red and blue shift, respectively. In a stress free silicon sample, optical phonons are triply degenerated due to cubic symmetry of Si crystal. However, the cubic symmetry will be broken and the triplet will be split by stress introduction in Si lattice [20, 21]. The resultant stress can be estimated from wavenumber shift ($\Delta\omega$) in Raman spectroscopy using Equation (4) [22]:

$$\sigma(MPa) \approx C \times \Delta\omega \quad (4)$$

where, C is a constant related to the elastic compliance and the deformation potential constant of the materials. Also C is dependent on stress direction and has different values for isotropic and biaxial stresses. This equation shows that a positive Raman shift (blue shift) indicates compressive stress, while a negative shift (red shift) shows tensile stress. A tensile stress was observed for PS layer with higher porosity. Higher porosity was observed in samples that were prepared using higher etching current densities which is due to higher rate of Si atomic removal. Removing Si atoms from Si atomic structure causes tensile stress in atomic structure as a

result of Si lattice constant expansion in PS structure. Thus, cracks in interconnections of pores in sample d can be due to a great stress induced in PS structure [23]. It can be discussed that as a result of residual stress in PS, strength in these samples reached yield point and led to fracture in PS structures which were fabricated with higher current densities, as shown in SEM planar view.

The effect of current density on the band gap structure (E_g) and emission properties of the PS samples was studied using PL spectroscopy. Here, in order to record S-band transition, excitation wavelength of PL was selected to be 405 nm. Fig. 5 shows the PL spectra of PS samples. Non-porous silicon sample did not show any emission within 200-1100 nm due to its indirect band gap ($E_g \sim 1.1$ eV) [24]. Increasing applied etching current densities from 10 to 80 mA.cm⁻² led to decrease in the emission peak towards shorter wavelength from 680 to 607.5 nm and also exhibiting visible luminescence in orange-red region of the spectrum.

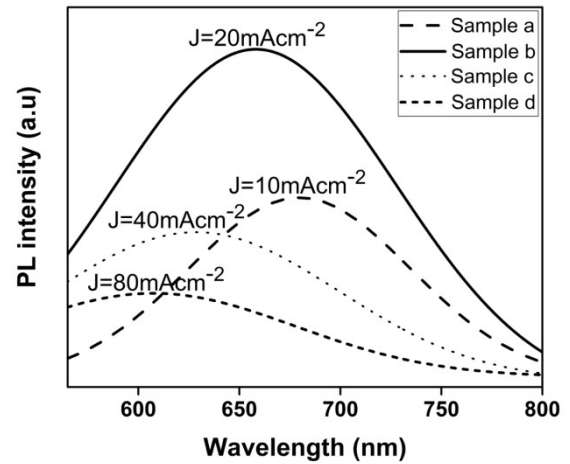


Figure 5. PL spectra of porous silicon samples with different current densities of 10, 20, 40, and 80 mA.cm⁻² for samples a , b , c and d , respectively

The PL blue shift for PS samples as a result of quantum confinement in PS nanocrystals confirms the decrease in crystallite size by increasing current density which is in good agreement with Raman spectroscopy [25]. The band gap energy values (E_g) corresponding to the PL peak positions are listed in Table 2. The results show that by increasing current density, the band gap of PS samples (with higher porosity) gets widened which is due to quantum confinement in Si nanocrystallites [26]. A remarkable increase in intensity of the emitted photon from porous samples was observed with initial increase in current density from 10 to 20 mA.cm⁻². Then a slight decrease in PL intensity was observed by increasing J from 20 to 80 mA.cm⁻². The PL properties of all samples are listed in Table 2. Maximum intensity was detected in sample b with $J=20$ mA.cm⁻², at wavelength of ~ 658.2 nm that can be due to formation of more Si

nanocrystallites in this sample compared to sample *a*. Applying higher current densities (more than 20 mA.cm⁻²) will increase dissolution of silicon material on the surface and depth (as shown in Fig. 2). Thus the luminescent crystallite density is reduced and PL intensity is diminished in samples *c* and *d* compared to sample *b*. Also the larger empty quasi-columnar macropores with long depth reduce the amount of nanocrystallites in PS nanostructure and would result in trapping the irradiated light in empty-macropores which would lead to decrease in PL intensities in samples *c* and *d*.

TABLE 2. Details of PL peaks for porous samples with different etching current densities

Samples	PL peak wavelength (nm)	PL peak intensity (a.u.)	FWHM	Bandgap (eV)
<i>a</i>	679.7	2340.6	129.0	1.82
<i>b</i>	658.2	4180.1	164.1	1.88
<i>c</i>	628.4	1916.4	166.3	1.97
<i>d</i>	607.2	1160.3	165.0	2.04

Fig. 6 shows the reflection spectra of PS samples compared with the c-Si sample. The maximum reduction in light reflection ranged from 450 to 800 nm was obtained for the PS samples with maximum porosity and larger micropores which evidently reduced the light reflection and increased the light-trapping. Thus sample *d* with the highest etching current density shows the lowest optical reflection which is due to the light-trapping properties in larger empty quasi-columnar macropores existing in this sample.

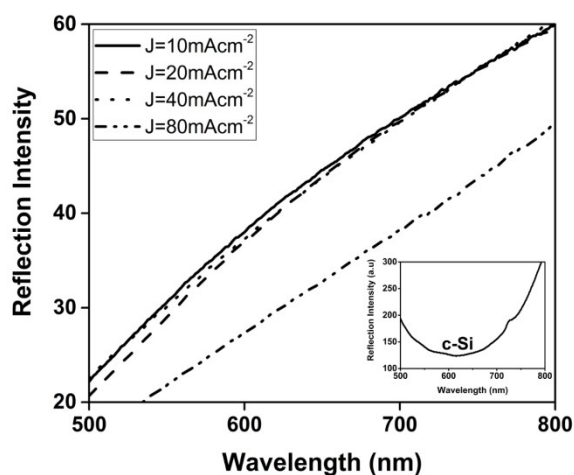


Figure 6. Absorption spectra of porous samples *a*, *b*, *c* and *d* compared with the c-Si sample

4. CONCLUSIONS

Porous silicon samples with different porous morphologies were synthesized using different etching

current densities (*J*) of 10, 20, 40, and 80 mA.cm⁻² through photo-assisted electrochemical etching method. Enlargement of quasi-columnar pore diameter and increase in thickness of porous layer were observed for the samples synthesized using higher etching current densities. The larger empty quasi-columnar macropores (with diameter of ~1– 4 μm) on the PS nanostructure led to decrease in pores density and diminishing the amount of luminescent Si nanocrystals in quasi-columnar silicon nanostructures surface which led to decrease in photon emission from this nanostructure. Also, larger empty quasi-columnar macropores in exposure of irradiated light trap caused a reduction in PL efficiency by light trapping. From the optical properties of the PS samples, it can be concluded that the porosity of PS is not the only parameter affecting the optical properties of porous samples. The morphology and size of the pores also play important role in optical properties such as luminescence behavior.

5. ACKNOWLEDGMENT

This work was supported by Materials and Energy Research Center [grant numbers 471394053].

REFERENCES

- Naderi, N., Hashim, M., Rouhi, J. and Mahmodi, H., "Enhanced optical and electrical stability of thermally carbonized porous silicon", *Materials Science in Semiconductor Processing*, Vol. 16, (2013), 542-546.
- Kumar, P., "Effect of silicon crystal size on photoluminescence appearance in porous silicon", *ISRN Nanotechnology*, Vol. 2011, (2011).
- Canham, L., "Porous Silicon Application Survey", *Handbook of Porous Silicon*, (2014), 733-740.
- Naderi, N., Hashim, M. and Amran, T., "Enhanced physical properties of porous silicon for improved hydrogen gas sensing", *Superlattices and Microstructures*, Vol. 51, (2012), 626-634.
- Naderi, N. and Hashim, M., "Porous-shaped silicon carbide ultraviolet photodetectors on porous silicon substrates", *Journal of Alloys and Compounds*, Vol. 552, (2013), 356-362.
- Massoudi, A., Azim-Araghi, M. and Asl, M.K., "Fabrication of P-Type Nano-porous Silicon Prepared by Electrochemical Etching Technique in HF-Ethanol and HF-Ethanol-H₂O Solutions", *Advanced Ceramics Progress*, Vol. 1, (2015), 24-28.
- Behzad, K., Yunus, W.M.M., Talib, Z.A., Zakaria, A. and Bahrami, A., "Effect of preparation parameters on physical, thermal and optical properties of n-type porous silicon", *International Journal of Electrochemical Science*, Vol. 7, (2012), 8266-8275.
- Ramesh, M. and Nagaraja, N., "Effect of current density on morphological, structural and optical properties of porous silicon", *Materials Today Chemistry*, Vol. 3, (2017), 10-14.
- Yaakob, S., Bakar, M.A., Ismai, J., Bakar, N. and Ibrahim, K., "The formation and morphology of highly doped N-type porous silicon: effect of short etching time at high current density and evidence of simultaneous chemical and electrochemical dissolutions", *Journal of Physical Science*, Vol. 23, (2012), 17-31.

10. Yaohu, L., Zhigang, Z., Jinchuan, G., Ji, L. and Hanben, N., "Disordered wall arrays by photo-assisted electrochemical etching in n-type silicon", *Journal of Semiconductors*, Vol. 37, (2016), 106001.
11. Das, M., Nath, P. and Sarkar, D., "Influence of etching current density on microstructural, optical and electrical properties of porous silicon (PS): n-Si heterostructure", *Superlattices and Microstructures*, Vol. 90, (2016), 77-86.
12. Gómez-Barojas, E., López-Hernández, O., Flores-Gracia, F., Tepal-Prisco, J., Silva-González, J. and Sánchez-Mora, E., "Study of morphological and optical properties of porous silicon", *Journal of Superconductivity and Novel Magnetism*, Vol. 26, (2013), 2219-2222.
13. Salman, K.A., Hassan, Z. and Omar, K., "Effect of silicon porosity on solar cell efficiency", *International Journal of Electrochemical Science*, Vol. 7, (2012), 376-386.
14. Aziz, W.J., Ramizy, A., Ibrahim, K., Hassan, Z. and Omar, K., "The effect of anti-reflection coating of porous silicon on solar cells efficiency", *Optik-International Journal for Light and Electron Optics*, Vol. 122, (2011), 1462-1465.
15. Ramizy, A., Aziz, W.J., Hassan, Z., Omar, K. and Ibrahim, K., "The effect of porosity on the properties of silicon solar cell", *Microelectronics International*, Vol. 27, (2010), 117-120.
16. Guozheng, W., Li, C., Xulei, Q., Ji, W., Yang, W., Shencheng, F. and Qingduo, D., "Influence of etching current density on the morphology of macroporous silicon arrays by photo-electrochemical etching", *Journal of Semiconductors*, Vol. 31, (2010), 074011.
17. Faraci, G., Gibilisco, S., Russo, P., Pennisi, A.R. and La Rosa, S., "Modified Raman confinement model for Si nanocrystals", *Physical Review B*, Vol. 73, (2006), 033307.
18. Piscanec, S., Cantoro, M., Ferrari, A., Zapien, J., Lifshitz, Y., Lee, S., Hofmann, S. and Robertson, J., "Raman spectroscopy of silicon nanowires", *Physical Review B*, Vol. 68, (2003), 241312.
19. Saxena, S.K., Borah, R., Kumar, V., Rai, H.M., Late, R., Sathe, V., Kumar, A., Sagdeo, P.R. and Kumar, R., "Raman spectroscopy for study of interplay between phonon confinement and Fano effect in silicon nanowires", *Journal of Raman Spectroscopy*, Vol. 47, (2016), 283-288.
20. Sahu, G., Sahu, V. and Kukreja, V., "Observation of low energy acoustic phonon modes at low temperature from stressed Si nanoclusters", *Materials Research Express*, Vol. 2, (2015), 025008.
21. Iatsunskiy, I., Nowaczyk, G., Jurga, S., Fedorenko, V., Pavlenko, M. and Smyntyna, V., "One and two-phonon Raman scattering from nanostructured silicon", *Optik-International Journal for Light and Electron Optics*, Vol. 126, (2015), 1650-1655.
22. Zhen-Kun, L., Yi-Lan, K., Ming, H., Yu, Q., Han, X. and Hong-Pan, N., "An experimental analysis of residual stress measurements in porous silicon using micro-Raman spectroscopy", *Chinese Physics Letters*, Vol. 21, (2004), 403-405.
23. Manotas, S., Agulló-Rueda, F., Moreno, J., Ben-Hander, F. and Martínez-Duart, J., "Lattice-mismatch induced-stress in porous silicon films", *Thin Solid Films*, Vol. 401, (2001), 306-309.
24. Naderi, N. and Hashim, M., "A combination of electroless and electrochemical etching methods for enhancing the uniformity of porous silicon substrate for light detection application", *Applied Surface Science*, Vol. 258, (2012), 6436-6440.
25. Rahim, A., Farhanah, A., Abdullah, M.S., Mahmood, A., Ali, N.K. and Zahidi, M.M., "Quantum Confinement of Integrated Pulse Electrochemical Etching of Porous Silicon for Metal Semiconductor Metal Photodetector", *Materials Science Forum*, Vol. 846, (2016), 245-255.
26. Hussein, M.J., Yunus, W.M.M., Kamari, H.M., Zakaria, A., Oleiw, H.F., "Effect of current density and etching time on photoluminescence and energy band gap of p-type porous silicon", *Optical and Quantum Electronics*, Vol. 48, (2016), 1-8.